Creep response of Ti–6Al–4V alloy produced by additive manufacturing: Effect of annealing at 1050 °C

PRE-PRINT (SUBMITTED COPY)

Creep response of Ti–6Al–4V alloy produced by additive manufacturing: effect of annealing at 1050 °C

S. Spigarelli[1], C. Paoletti[2*], E. Cerri[3], E. Santecchia[1,*], M. Cabibbo[1]

1. DIISM, Università Politecnica delle Marche, via Brecce Bianche, 60131 Ancona, Italy

2. Faculty of Engineering, Università degli Studi eCampus, Via Isimbardi 10, 22060 Novedrate, Italy

3. DIA Università di Parma, V.le G. Usberti 181/A, 43124, Parma, Italy

*E. Santecchia: corresponding author

Received 1 August 2022, Revised 17 October 2022, Accepted 31 October 2022, Available online 5 November 2022, Version of Record 10 November 2022.

https://doi.org/10.1016/j.msea.2022.144278

Abstract

Herein, the creep response of a Ti–6Al–4V alloy produced by additive manufacturing and subsequently annealed at 1050 °C is investigated at temperatures ranging from 500 to 650 °C. The heat treatment produces the typical Widmanstätten microstructure with thin β-lamellae interposed between coarse α-lamellae. The minimum creep rates observed in this study are lower than those previously obtained by testing the same material after annealing at 740 °C. The minimum creep rate dependence on the applied stress and temperature is compared with literature data of tests of alloys with Widmanstätten microstructures produced by traditional technologies. A modified form of a previously developed constitutive equation is proposed. This equation successfully described the creep responses of traditional equiaxed and duplex Ti–6Al–4V alloys and of the same material produced by additive manufacturing and subsequently annealed at 740 °C. The suggested modification introduces a threshold stress, which is related to the presence of finely spaced α–β interfaces and α_2-Ti_3Al particles. This threshold stress is considered to be negligible when the distance between the α–β interfaces is long and the α_2-Ti_3Al particles are absent or excessively spaced. In contrast, in the materials with Widmanstätten microstructures, even minor differences in the heat treatment conditions and/or the processing history cause considerable variations in the distance between the α–β interfaces. This coupled with the occasional precipitation of α_2-Ti_3Al particles results in different threshold stress values.

1. Introduction

Ti–6Al–4V alloy is a commercial material well suited for processing by additive manufacturing. In particular, selective laser melting (SLM), also known as laser-beam powder-bed fusion, is an excellent candidate for industrial-scale production of Ti–6Al–4V components. Consequently, several recent studies, accurately reviewed by Liu and Shin [1], thoroughly investigated the microstructural features and mechanical properties of the additively manufactured (AM) alloy. Notably, the creep response of the AM alloy has not received equal attention. Thus, in a previous study all recently available data on the creep behaviour of Ti–6Al–4V produced by different technologies and having different initial microstructures were collected [2]. Moreover, they were compared with new experimental results obtained by testing a Ti–6Al–4V alloy produced by SLM and subsequently

annealed at 740 °C for 130 min. Furthermore, an additional effort was made to rationalise the creep responses of the alloys produced by traditional technologies and AM, respectively. This analysis demonstrated that the same equation can be successfully used to describe the creep response of Ti–6Al–4V alloy, irrespective of the initial microstructure and the production technique. The minimum strain rate ($\dot{\varepsilon}_m$) dependences on the stress (σ) and temperature (T) of "traditional" materials with both equiaxed and duplex microstructures and annealed or as-deposited AM alloys were expressed by

$$\dot{\varepsilon}_m = A\frac{D_0 Gb}{kT}\left(\frac{\sigma_\rho}{G}\right)^3 exp\left(\frac{\sigma_\rho b^3}{kT}\right) exp\left\{-\frac{Q_L}{RT}\left[1-\left(\frac{\sigma_\rho}{R_{max}}\right)^2\right]\right\}, \quad (1)$$

where b was the Burgers vector; G was the shear modulus; k was Boltzmann's constant; A was a constant, and D was the self-diffusion coefficient, which was expressed as:

$$D = D_0 exp\left(-\frac{Q_L}{RT}\right), \quad (2)$$

where D_0 was a material parameter and Q_L was the activation energy (for lattice self-diffusion in pure metals). The σ_ρ term (dislocation hardening) was calculated by handling the equation:

$$\sigma = \sigma_\rho + \sigma_{ss} = \sigma_\rho + \delta\sigma \quad (3)$$

where σ_{ss} was the solid solution strengthening term and δ is a constant (= 0.4) introduced to represent its effect.

The R_{max} parameter (maximum strength) was expressed as

$$R_{max} = 1.5UTS\frac{G_T}{G_{RT}}, \quad (4)$$

where G_{RT} and G_T were the shear moduli at room temperature and the testing T, respectively.

For any interested reader, the literature data, genesis, and use of Equations (1)–(4) are described in detail in [2]; hence, in the present study, they were not extensively discussed. However, an important issue, already presented in [2] worth describing here is the extremely large scatter of the minimum creep rate data observed when comparing different batches [3–8] of Ti–6Al–4V alloys having Widmanstätten structures. This peculiar microstructure forms after annealing the alloy above the β-transus temperature and subsequently cooling at a relatively high cooling rate. Equations (1)–(4) provide curves that bisect the 'clouds' of experimental data; however, the scatter is extremely large to

conclude that the model is perfectly adequate for describing the creep response. This discrepancy suggests broadening the study on the creep response of AM Ti–6Al–4V by also annealing the alloy at 1050 °C, which is well above the β-transus temperature, to obtain a Widmanstätten structure. A few creep results at 650 °C, a temperature above the predictable range of α_2-Ti_3Al precipitation, have recently been reported by the authors of the present study [9]. The aim of that preliminary investigation was limited to comparing the creep responses of the alloy with a Widmanstätten structure before and after annealing below the β-transus temperature. The experimental results proved that at this temperature, the alloy with a Widmanstätten microstructure exhibited lower creep rates than after annealing at 704 or 740 °C. This behaviour cannot be explained by Equations (1)–(4), in particular, owing to the ultimate tensile strength (UTS) of the alloy annealed above the β-transus temperature being slightly lower than that of the material annealed at 704–740 °C. These observations indicated the need to enlarge the range of the experimental conditions to be investigated to cover the full temperature range considered in [2]. Thus, the aim of the present study was twofold: i) present a much more extensive set of experimental data obtained by testing the AM alloy annealed at 1050 °C at different temperatures by both constant-load and variable-load creep experiments (CLEs and VLE, respectively) and ii) provide a model on a wider scale applicable to alloys produced by traditional technologies and able to describe the creep response of Ti–6Al–4V with a Widmanstätten structure. Therefore, the present study reports new data on the creep responses at 500 and 600 °C of the AM Ti–6Al–Ti-6Al-4V annealed at 1050 °C. Moreover, based on the findings presented in [2], it provides supplementary material in form of additional microstructural analyses.

2. Material and Experimental procedures

2.1 Material and sample production

In this study, commercial gas-atomised Ti–6Al–4V grade 23 extra-low-interstitial powders (5.5–6.5 % Al, 3.5–4.5 % V, 0.25 % F, 0.1 % O, 0.05 % maximum N, 0.08 % maximum C, 0.011 % maximum H, and Ti balance wt.%) were used. The powder particles had sizes ranging from 15 μm to

45 μm. An SLM280 machine (SLM Solutions AG, Lübeck, Germany) equipped with a 400 W IPG fibre laser was used for the production of dog-bone creep samples, with a square section of area A_0 = 3 mm × 3 mm and a 25 mm gauge length. A powder bed was preheated at 80 °C, and deposition was performed in argon (Ar) to reduce oxygen concentration to 0.05 %. The building direction was parallel to the gauge length of the specimen. The deposition was conducted to a thickness of 60 μm at a scanning speed of 1250 mm/s, with hatch spacing of 120 μm, and laser power of 340 W. The post-processing treatment consisted of annealing at 1050 °C, which is well above the β-transus temperature, for 1 h, followed by cooling in Ar at 0.4 °C/s. This relatively slow cooling was expected to lead to the formation of a Widmanstätten structure with reduced internal stress [10]. Both sample production and post-processing heat treatment were performed by BEAMIT (https://www.beam-it.eu/, Fornovo di Taro 43045, Italy).

2.2 Creep experiments

CLEs and VLEs were conducted at 500, 600, and 650 °C in air on samples whose surfaces were in the as-deposited state. In a CLE, a load P was applied immediately after a short soaking time at the testing temperature and maintained until rupture or test interruption in the tertiary stage. In a VLE, a sample was loaded similarly to in a CLE under a given initial stress; however, after the minimum creep rate range was presumably attained, the load was abruptly changed.

The soaking time at temperature before loading was typically 0.5–1 h, except before a CLE test, in which the soaking time was 145 h.

The test temperature was measured using four thermocouples, and the elongation was continuously measured using a linear variable displacement transducer.

2.3 Room-temperature mechanical properties

To evaluate the UTS, tensile tests at room temperature were performed on samples having the geometry of a creep experiment specimen. The surfaces of the samples used for the tensile tests were

in the as-deposited state. The test strain rate was 3×10^{-2} s^{-1}. The UTS after heat treatment at 1050 °C was 922 ± 2 MPa.

Rockwell hardness (HRC) tests were performed on as-heat treated and crept sample heads. Because these tests were merely aimed at assessing the age-hardening responses of the alloy, the hardness was measured in these (almost) unstressed portions of the samples. The dislocation substructures introduced by loading and straining considerably influenced the hardness of the gauge lengths, thus masking the possibly considerably limited effects of age hardening. The HRC value after heat treatment was 38.1 ± 0.5 for the alloy after annealing.

2.4 Microscopy

Samples for light microscopy analyses were mechanically ground and polished with a colloidal suspension and subsequently etched using Kroll's reagent (100 mL H_2O + 2 mL HF + 4 mL HNO_3). Following this, the samples were observed under a Leica DMi8 optical microscope (Germany). Scanning electron microscopy (SEM) observations were conducted using a Tescan Vega 3 scanning electron microscope (Brno, Czech Republic) at an accelerating voltage of 30 keV.

For transmission electron microscopy (TEM) analyses, thin foils were obtained from untested and crept sample heads. The samples were prepared by mechanical grinding and polishing to a thickness of 150 µm. This was followed by twin-jet electro-polishing to reach 60 µm thickness using a Struers™ Tenupol-5® device (Struers Inc., Westlake, Cleveland, OH, USA) with a solution consisting of 5 % perchloric acid, 35 % butanol, and 60 % methanol at −35 °C and voltage V = 24 V. The discs were dimpled to a reach a thickness of 20–25 µm and ion-milled to electron transparency using a Gatan© precision ion polishing system (Gatan Inc., Pleasanton, CA, USA) operating at 8 keV (incident beam angle progressively reduced to 8°, 6°, and 4°). The TEM analyses were performed using a Philips™ CM-20 microscope (Philips It, Milano, Italy) working at 200 kV and equipped with a double-tilt liquid nitrogen cooling specimen holder. Selected area diffraction patterns (SAEDPs) were recorded using a converged beam. Based on the SAEDPs, The crystallographic structures of the

α, α′, and α_2-phases were found to have α-[0001] or α-[$2\bar{1}\bar{1}0$] directions parallel to the beam direction.

3. Results

3.1 Initial Microstructure

Figure 1 shows the initial microstructure of an annealed SLM-manufactured-alloy (referred as SLM-alloy) (light microscopy and SEM images). A Widmanstätten microstructure is noticeable as thin layers of light α-phase-decorating prior β-grains.

Figure 2 shows a representative TEM micrograph of the annealed SLM-alloy. The microstructure consists of thin and long β-lamellae interposed between much thicker α-lamellae. The thicknesses of the β and α-lamellae are in the ranges of 110–140 and 390–460 nm, respectively. In addition, remote α'-martensite colonies having essentially the same thickness as the α-lamellae are uniformly distributed in the α-phase of the Widmanstätten microstructure.

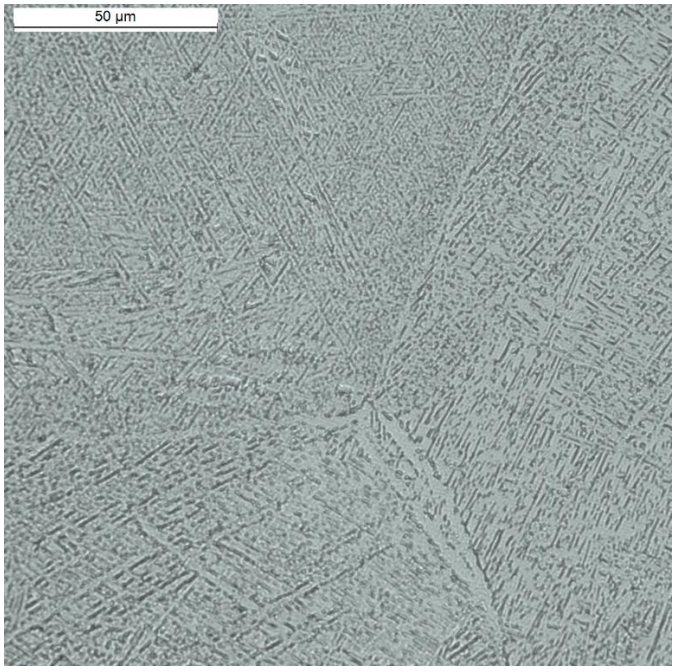

a)

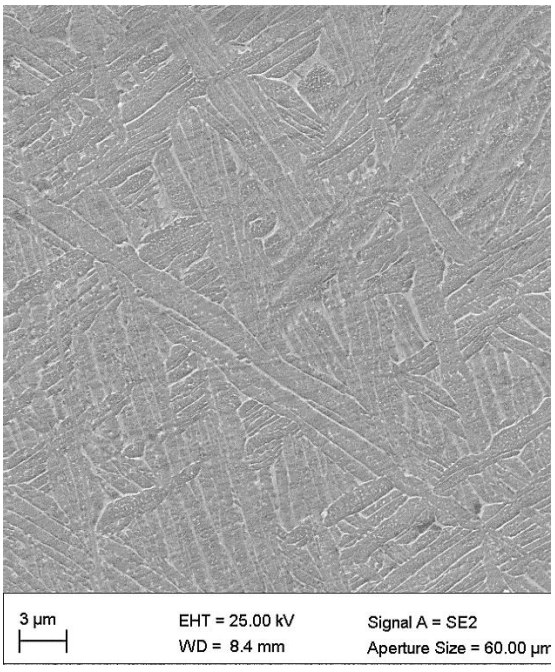

b)

Figure 1. Microstructure of SLM-alloy after annealing at 1050 °C observed by a) optical microscopy and b) SEM.

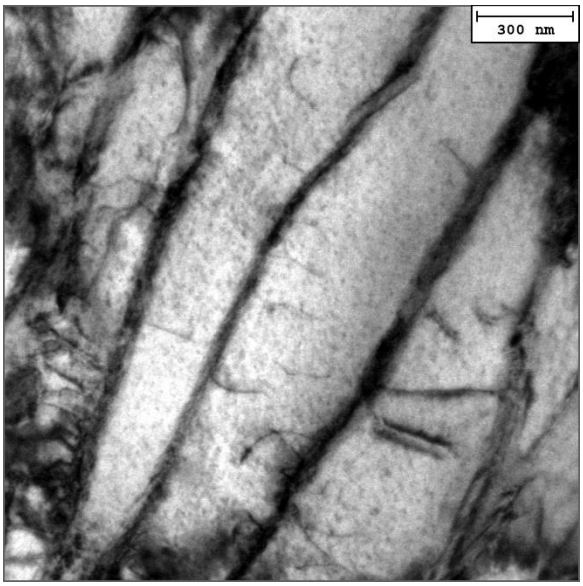

Figure 2. Microstructure of SLM-alloy after annealing at 1050 °C observed by TEM.

3.2 Creep response

Figure 3 shows the strain rate versus strain creep curves obtained in the present study at 500 and 600 °C (from CLEs and VLEs). Figure 4 displays the creep curves at 650 °C from [9] and supplemented by one additional VLE curve obtained in this study at this temperature. Figure 4b compares the curves obtained after short (0.5 h) and very long (145 h) soaking times at the testing temperature before loading.

In general, the shapes of the creep curves are similar to that observed when testing the alloy after annealing at 740 °C [2], and consist of a well-defined primary stage, a minimum creep rate range, and an extended tertiary stage. Figure 4b clearly shows that a long permanence at 650 °C before loading only results in a slight increase in the creep rates and a reduction in the strain to fracture.

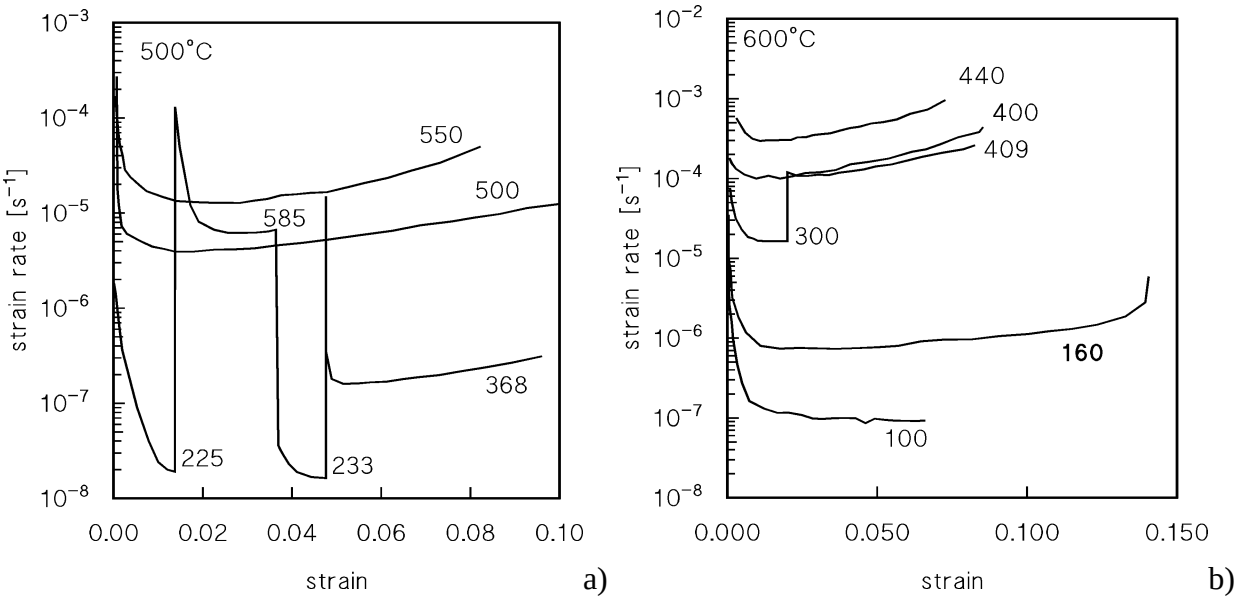

Figure 3. Strain rate versus strain creep curves from CLEs and VLEs at 500 and 600 °C of AM alloy annealed at 1050 °C. Numbers are nominal stresses in MPa. Test conducted under 100 MPa is interrupted.

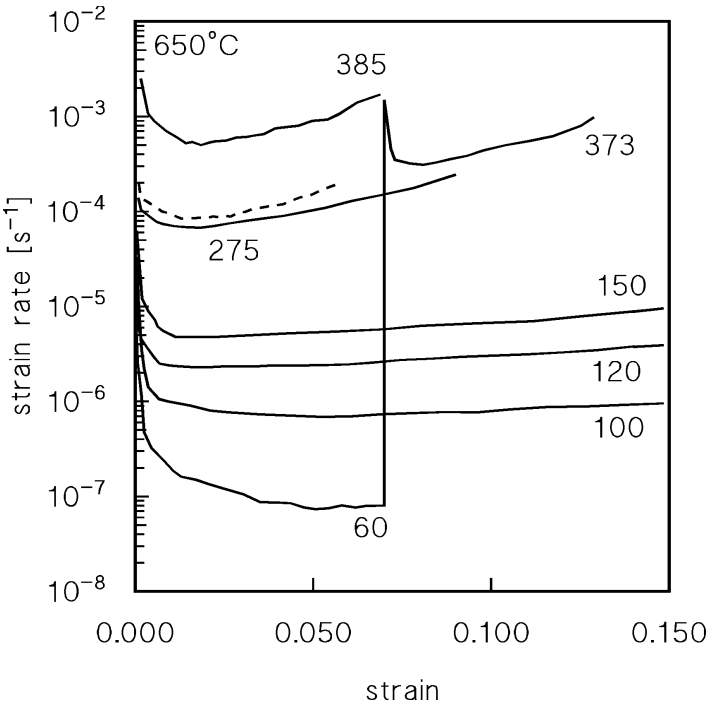

Figure 4. Representative strain rate verses strain creep curves from CLEs and VLEs at 650 °C of AM alloy annealed at 1050 °C [9]. Numbers are nominal stresses in MPa. Broken line corresponds to test conducted under 275 MPa after 145 h annealing prior to loading.

Figure 5 shows the minimum strain rate as a function of the applied stress; the experimental data approximately align on straight lines with slopes 7, 5.2, and 4.8 at 500, 600, and 650 °C, respectively. The data displayed in Figure 5 cover over three orders of magnitude of strain rates, and do not

present a large scatter; therefore, they present an excellent basis for the search of a reliable constitutive model.

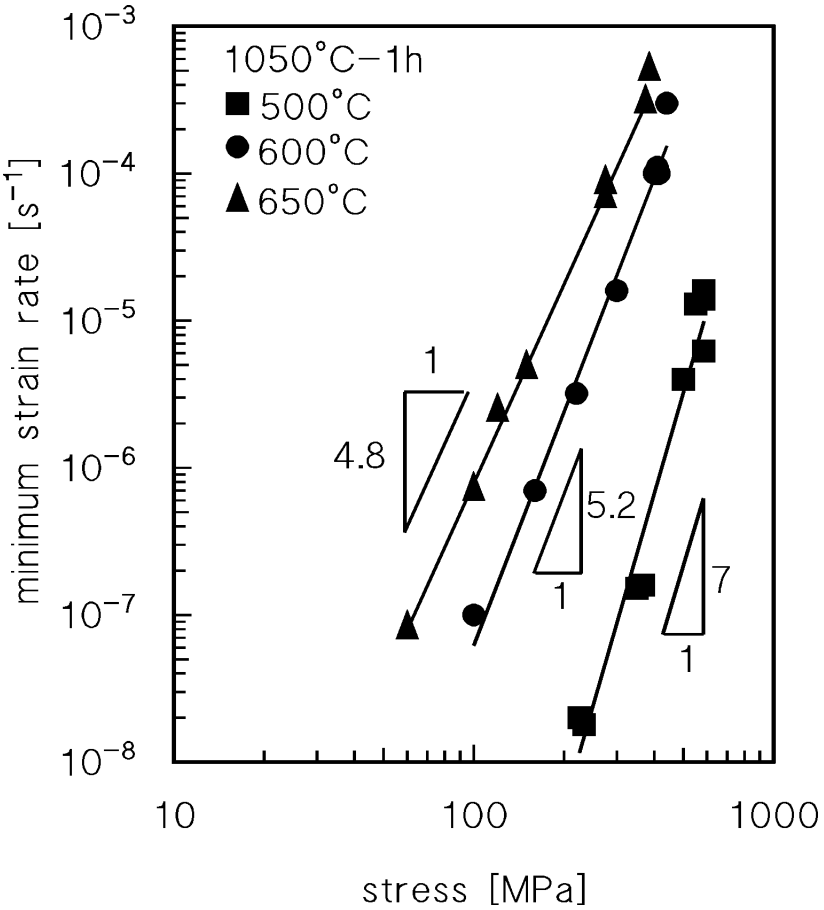

Figure 5. Minimum creep rate as function of applied (nominal) stress.

Figure 6a shows the data obtained in the present study and the literature data on alloys with Widmanstätten structures [3–8] produced by traditional technologies. The data obtained in this study cross the ‘cloud’ of the literature data. The drastic scatter of the latter causes occasionally a substantial deviation between the solid (this study) and open (literature) data points.

Figure 6b presents a comparison of the minimum creep rate measured in this study and those reported for the AM alloy annealed at 740 °C in [2]. As already noted in [9], compared to annealing at 740 °C, annealing at 1050 °C results in lower creep rates in the entire investigated stress and temperature ranges; however, the difference progressively vanishes in the high-stress regime.

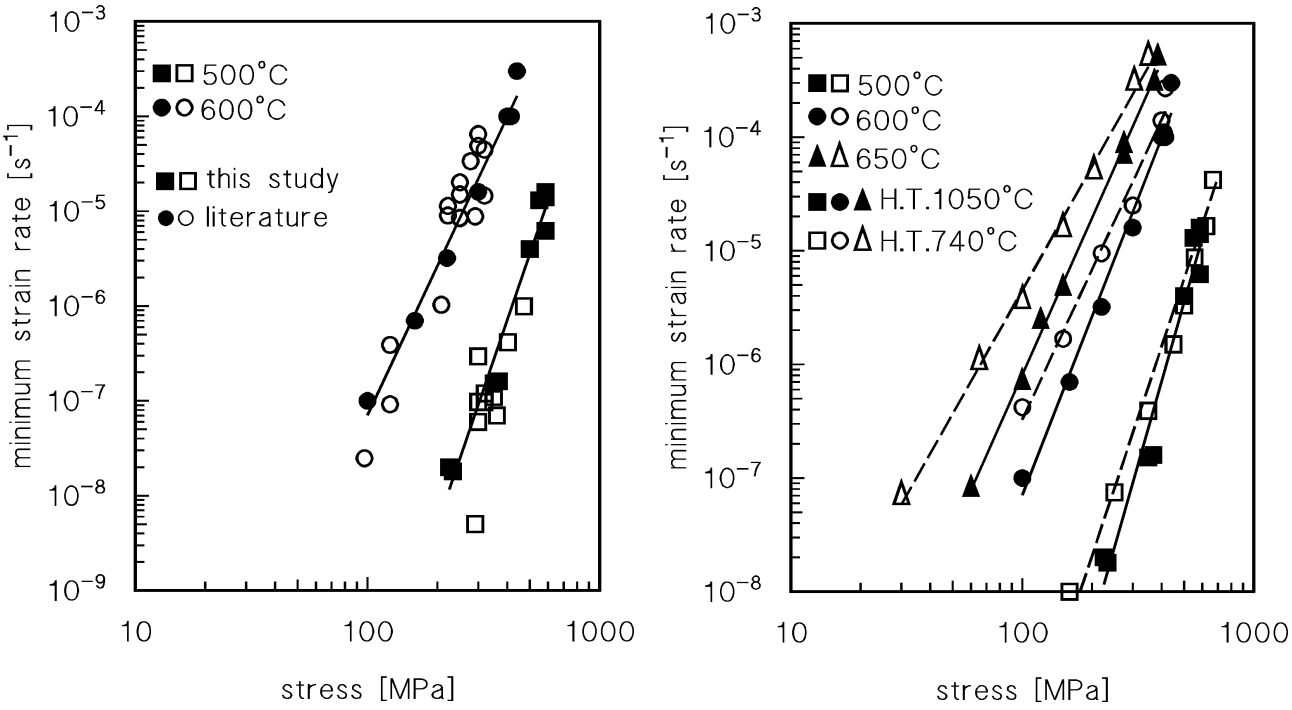

Figure 6. Comparison of data obtained in present study by testing AM alloy annealed at 1050 °C with a) literature data of traditionally processed Ti–6Al–4V with Widmanstätten microstructure [3–8] and b) data of same alloy produced by additive manufacturing and annealed at 740 °C [2].

3.3 Hardness after high-temperature exposure

Figure 7 shows the HRC measurement results of the heads of crept samples. The data approximately present curves typical of age-hardening materials. Although this behaviour does not necessarily fully represent the phenomena occurring in the gauge lengths, where the dislocation activity significantly affects the microstructural evolution, it can be considered of interest for the description of the present model. At 500 °C, the hardness increases above 200 h of exposure, a possible indication of α_2-Ti_3Al precipitation. At 600 and 650 °C, the hardness decreases for the sample heads after a long time of exposure. At 650 °C, the hardness continuously reduces with the time of creep exposure. Because the dislocation activity considerably alters the microstructural evolution in the gauge length, the hardness trend showed in Figure 7 cannot be used to qualitatively predict the creep response of the alloy. However, the results in Figure 7 remain significant as they show that the alloy is unstable at high temperatures. Permanence at high temperatures causes a moderate variation in the properties of the alloy, a phenomenon observed on a similar scale for the material annealed at 740 °C in [2].

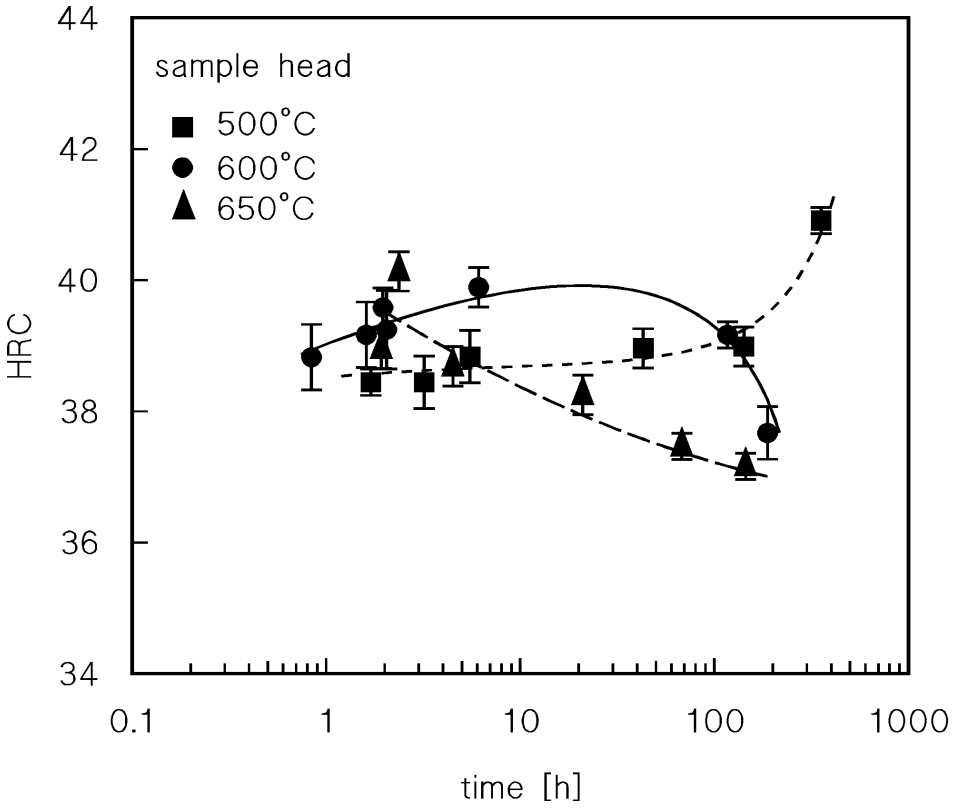

Figure 7. HRC hardness measured on crept sample heads.

3.4 Microstructure after creep experiments

Figures 8–10 show the microstructures of the crept samples observed using SEM and TEM. The most straightforward finding of the analysis shown in Figure 8 is the fragmentation of the β-lamellae at 650 °C. The micrographs obtained by TEM are more relatively interesting (Figures 9 and 10). They reveal that the microstructure of the alloy crept at 500 °C under an initial stress of 225 MPa (VLE in Figure 3a, at high-temperature exposure for 355 h) is still characterised by diffused long and thin β-lamellae (Figure 9a). Their thickness is approximately four times lower than those of the α-lamellae. Within the α-phase, the precipitation of α_2-Ti_3Al is evident (Figure 9b). This precipitated phase exists in the form of both long precipitates and much smaller cube-shaped particles, as presented in Figures 9b and 9c, respectively. The long particles have an average length of 450–480 nm and an average width of 55–60 nm, whereas the square-shaped particles are 180 nm in size. The dislocations bow around these particles, indicating a remarkable strengthening effect due to the dislocation–particle interactions

(Orowan bowing and/or climbing above the particles). The formation of the α_2-Ti_3Al phase, as also reported by other studies (see [11]), is expected, because the testing temperature is in the range where its precipitation is probable. The crystallographic relationship between the α_2 and α-phases is found to be was α_2-$[01\bar{1}1] \parallel \alpha$-$[01\bar{1}1]$, as shown in the insets of Figures 9b and c.

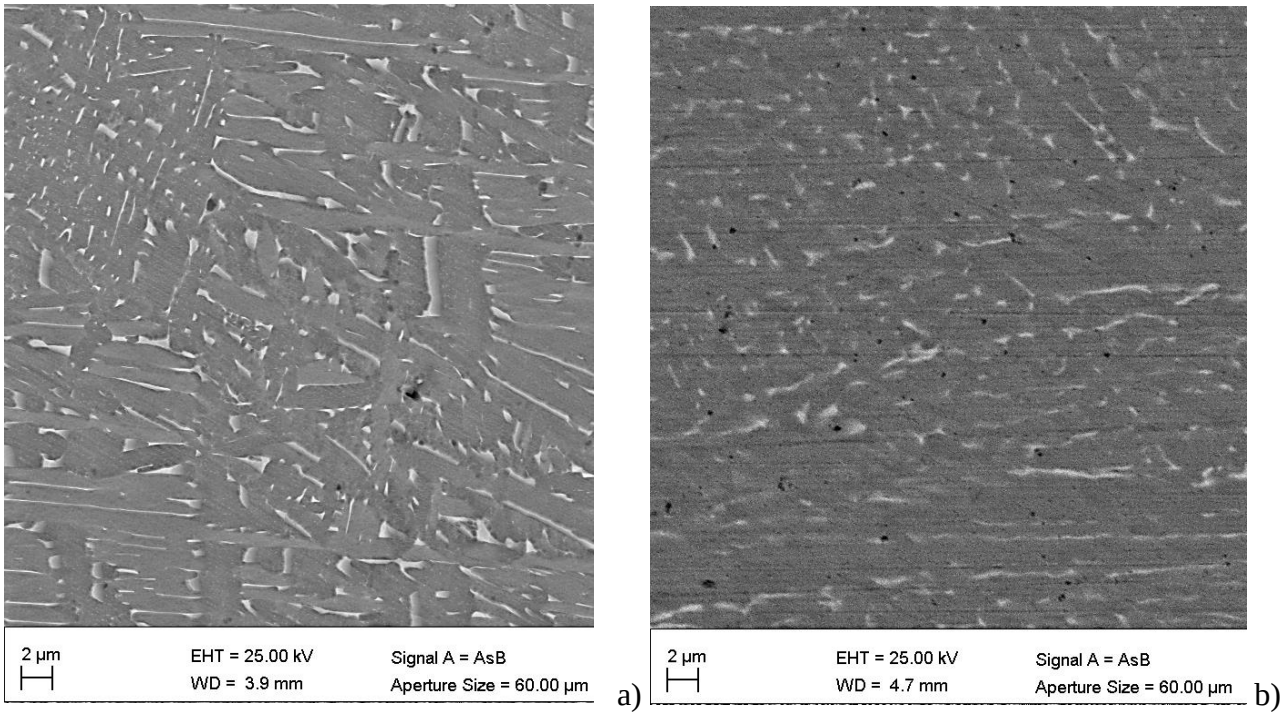

Figure 8. SEM micrographs of samples tested at 650 °C/275 MPa (a) and 650 °C/60 MPa (b).

Another distinctive microstructural feature is the β-lamellae fragmentation phenomenon, as shown in Figure 9d. It is activated by long holding times at high temperatures, as noticeable in Figures 8 and 9d, and has been described in other studies [10]. The dislocation activity due to creep straining is ultimately responsible for the progressive β-lamellae fragmentation.

The lamellar microstructure of the alloy crept at 650 °C under an initial stress of 60 MPa (VLE in Figure 4a, total exposure time of 187 h) is shown in Figures 8b and 10a. In particular, in the α-phase, dislocation sliding primarily occurs along $\boldsymbol{g} = (0002)$ and $\boldsymbol{g} = (0\bar{1}10)$ [13], as shown in Figure 10b. These two sliding directions form a local network of dislocations. Similar results have been reported by Li *et al.* [11].

Occasionally, α'-martensite colonies are still observed. Dislocation accumulation occurs in the α′ to α lath interfacial region owing to local strain accommodation followed by both β to α and β to α′-phase transformations. Stacking faults (SFs) are formed in the α-lamellar structures, which was also reported by Li et al. [11] and Su et al. [14].

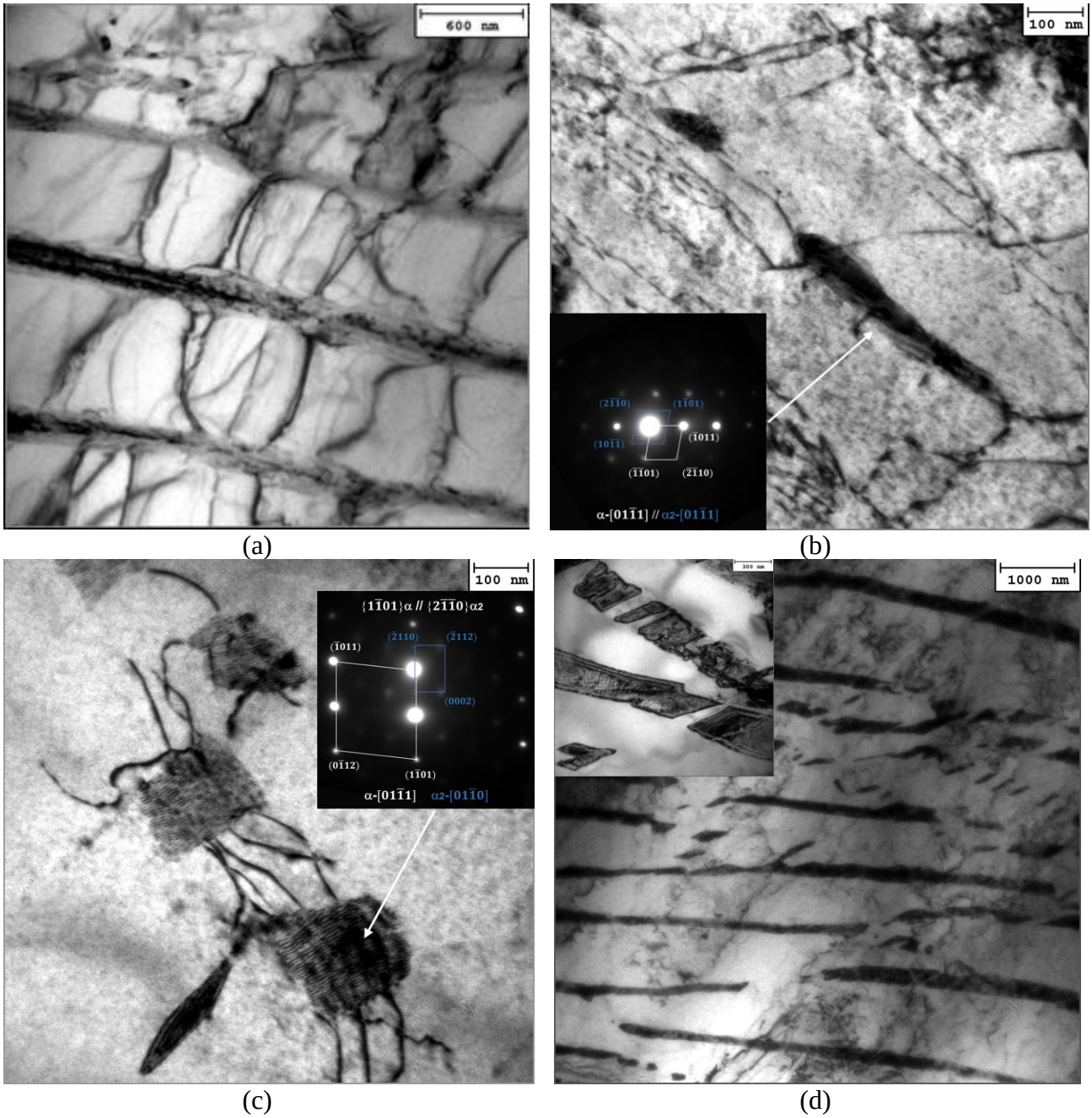

Figure 9. TEM micrographs of 500 °C/225 MPa crept sample showing (a) alloy α–β lamellar microstructure, α_2-Ti_3Al phase formation with long-thin morphology (b), and small particles with square morphology (c), and (d) β-lamellae fragmentation. Insets of (b) and (c) show SAEDPs of α_2-Ti_3Al; inset of (d) show details of some fragmented β-lamella.

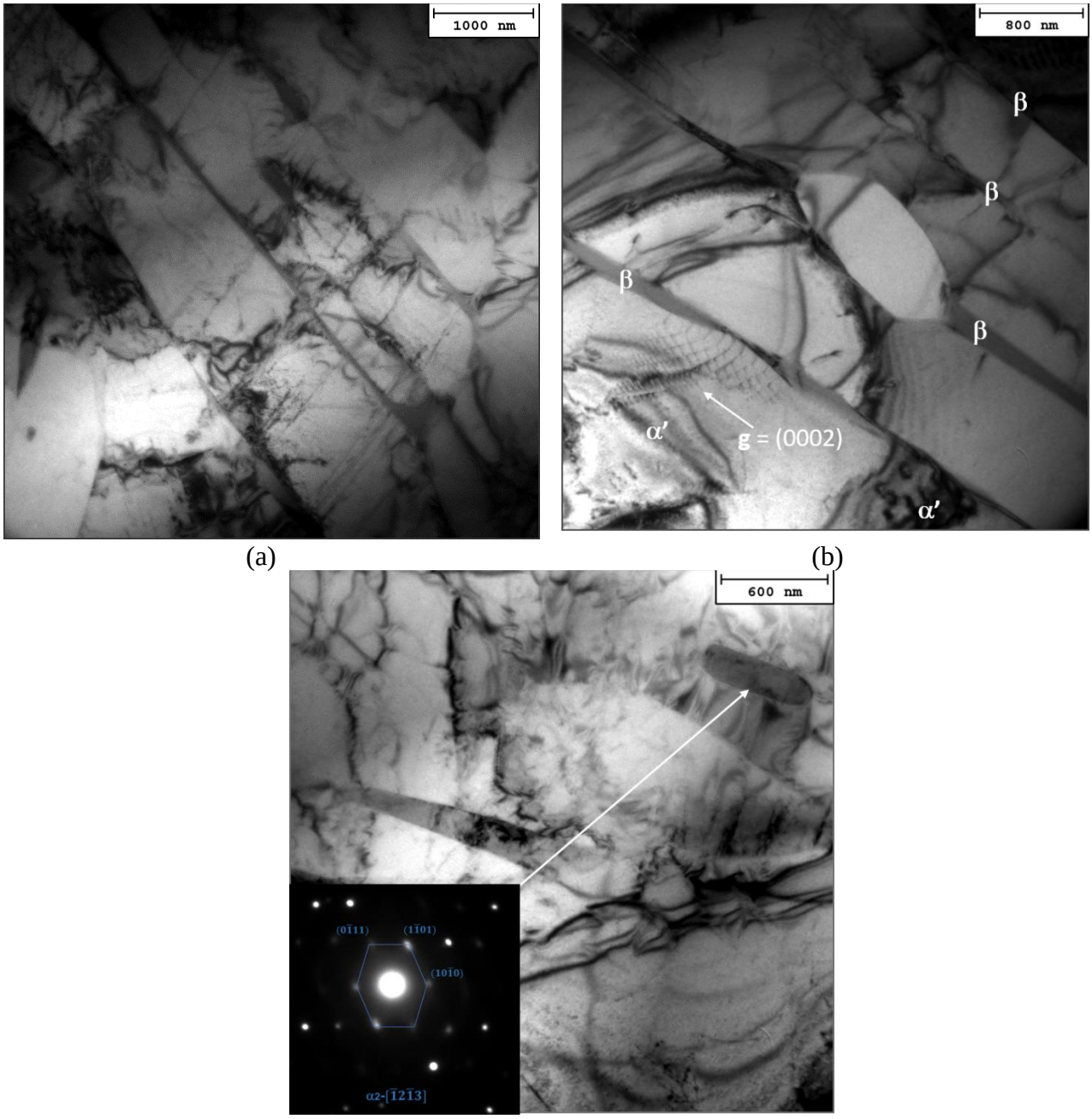

Figure 10. TEM micrographs of VLE sample tested at 650 °C under initial stress of 60 MPa, showing (a) α–β lamellar morphology, (b) tangled dislocations with wave-like sliding interactions, and (c) α_2-Ti_3Al phase and related indexed SAEDP (inset).

The presence of quite coarse α_2-Ti_3Al particles is also observed in the sample crept at 650 °C (Figure 10c). The Ti_3Al particles are ovoid in shape (120–150 nm in width and 600–800 nm in length). The crystallographic relationship between the α_2 and α phases was found to be α_2-$[2\bar{1}\bar{1}0]$ // α-$[2\bar{1}\bar{1}0]$ with α_2-$(0\bar{1}11)$ // α-(0001) crystallographic direction.

A quantitative evaluation of the β, α′, α_2, and α-phases in the samples annealed at 1050 °C and crept at 500 °C/60 MPa and 650 °C/225 MPa is reported in Table I.

Table I. Volume fractions (% vol.) of β, α′, α_2, and α-phases in VLE samples crept at 650 °C/60 MPa (initial stress) and 500 °C/225 MPa.

crept sample	β	α’	α_2	α
500 °C and 225/577/233/368 MPa	~12.0	~2	~0.15	bal.
650 °C and 60/373 MPa	~9.5	~1	~0.08	bal.

4. Discussion

4.1 Microstructural features of annealed Ti–6Al–4V produced by AM: context

Section 3 provides interesting information on the creep response of the AM Ti–6Al–4V alloy annealed at 1050 °C and the microstructures of the crept samples. The better creep response of the alloy annealed at 1050 °C than that of the alloy annealed at 740 °C is evident. Any rationalisation of this difference in the creep response should be based on a comparative analysis of the microstructural features.

It is widely known that the α–β phase transformation of a Ti–6Al–4V alloy strongly depends on the annealing temperature and the cooling rate. The equiaxed microstructure, obtained for example by a long annealing (6 h) at 850 °C followed by air cooling [3], consists primarily of α-grains surrounded by a much smaller volume fraction of finer β-grains. The duplex microstructure is characterised by the co-presence of equiaxed α- and lamellar α + β-grains. For example, colonies of α-lamellae, with an inter-lamellar small fraction of a retained vanadium-rich β-phase, form with equiaxed α-grains after annealing at 950 °C for 2 h, followed by air cooling to 700 °C [3]. Finally, annealing above the β-transus temperature followed by cooling at a relatively high cooling rate promotes the formation of a fine Widmanstätten structure.

The abovementioned microstructural evolution with thermal history is important as it considerably affects the mechanical properties, particularly at room temperature [15–17]. This is particularly for AM

Ti–6Al–4V alloys [18]. During the additive manufacturing process, cooling rates can be as high as 10^6 °C/s [18]. Such cooling rates inhibit the complete α–β phase transition, and the bcc β-phase decomposes by martensitic diffusionless transformation, leading to the formation of α′-martensite in the as-synthesised condition. The α'-martensite forms as fine needles and has a high dislocation density. The co-presence of α-grains, α′-needles, and a possible small volume fraction of intergranular β-lamellae is the cause of the strong microstructural anisotropy. The size and morphology of the α′-martensite and its crystallographic orientation, which is closely related to the prior β-grain orientations, affect the room-temperature mechanical properties of the AM alloy. The presence of α′-martensite in AM Ti–6Al–4V alloys results in high strength and poor ductility. Thus, post-processing heat treatments are needed to increase the ductility, inducing simultaneously a slight reduction in the alloy yield strength. To completely decompose α'-martensite to achieve a significant ductility improvement, the heating temperature should reach 800 °C for a typical minimum duration of 6 h [18–22].

4.2 Microstructure of Ti–6Al–4V during creep exposure: recalling effect of annealing at 740 °C

The findings obtained by TEM analysis of the sample crept after annealing at 740 °C in [2] are recalled for completeness. Additional micrographs are also discussed in this section to provide a sound basis for a reasonable interpretation of the material behaviour after annealing at 1050 °C.

Significant microstructural differences between the samples tested at 500 °C and 160/667 MPa (VLE) and those crept at 600 and 650 °C under 100 MPa (CLE) were observed in [2]. In particular, the microstructure of the sample tested at 500 °C after 476 h still showed a noticeable amount of α′-martensite in the α-grains. The volume fraction of the α-grains containing α′-martensite accounted for approximately 25 % volume. In fact, the α′-phase still present in these grains was only a small fraction of the grain volume; hence, the total amount of α′-martensite did not exceed 8–10 %. α′-martensite nucleated in the form of fine acicular structures at the prior β-grain boundaries, from which it grew within the α-grains being formed during rapid cooling by the SLM. The typical spatial configuration of different individual α′-colonies mostly consisted of chessboard structures. Both the α and α′-phases

had the same hcp crystallographic structure with minimal lattice differences. In contrast, the chessboard structures were observed to have a fixed crystallographic orientation relationship with the hosting α phase, being approximately ±45° with respect to α. Crystallographic relationships between the different detected phases were determined using SAEDPs (Figure 11).

The material crept under a low load, e.g., σ = 100 MPa, and a high temperature, e.g., 600 and 650 °C, contained an extremely small fraction of α′-martensite colonies in the α-phase and a small fraction of the β-phase (Figure 11b). In contrast, some traces of the β-phase (3 % by volume) were also detected in the sample tested at 500 °C. For clarity, the volume fractions of the β, α, and α′-phases in the three samples are listed in Table II.

Table II. Volume fractions (% vol.) of β, α, and α′ phases in VLE500, CLE600, and CLE650 samples.

Creep sample	β	α′	α
500 °C and 160/667 MPa	~3	~8	bal.
600 °C and 100 MPa	~4	<1	bal.
650 °C and 100 MPa	~8	<1	bal.

The reported amounts of the β-phase were not significantly different from those in the initial uncrept condition. The creep exposure did not considerably change the amount of the β-phase in the alloy. Regarding the size of the detected β-platelets, the typical lateral width (thickness) was 20 ± 4 nm, irrespective of the creep condition.

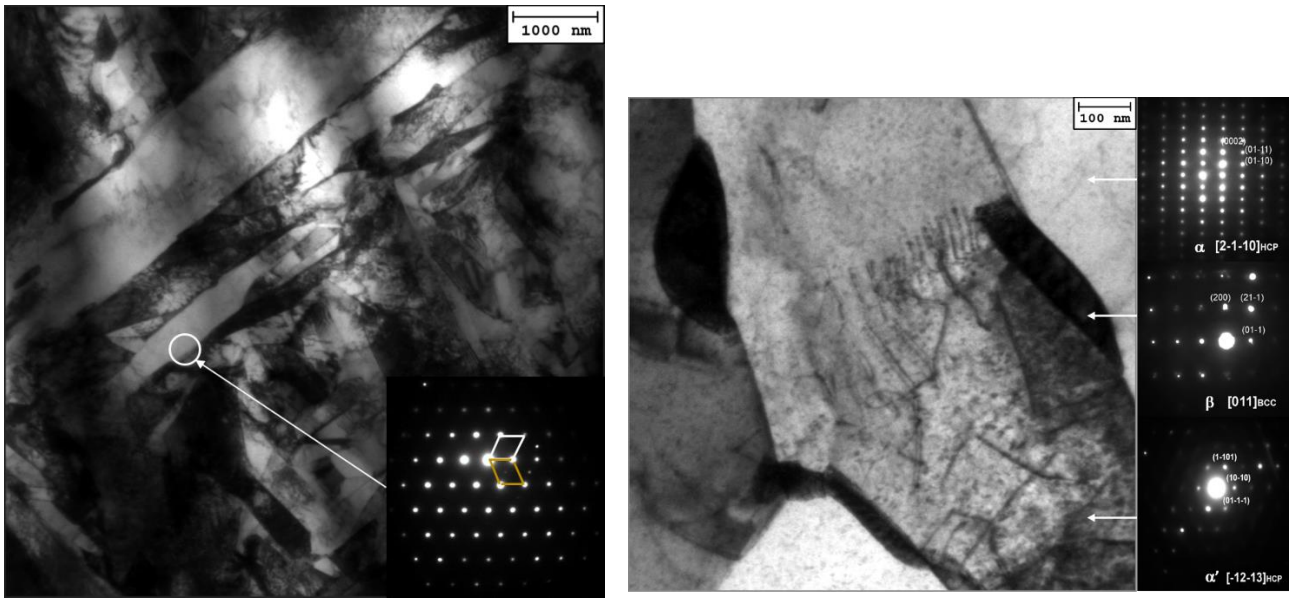

(a) (b)

Figure 11. Representative TEM microstructure of SLM-alloy after creep experiments: a) 500 °C and 160/667 MPa and b) 600 °C and 100 MPa. Insets of (b) show indexed SAEDPs of α, β, and α′ phases.

The experimental results showed that transformation of the retained α'-martensite occurred during creep exposure. Thus, it can be reasonably expected that higher exposure temperatures and longer durations can induce a complete α′ to α-phase transformation [23].

Based on these observations, creep response was considered in [2] to be is primarily driven by the deformation of the α-phase, which accounts for approximately 90 % of the overall alloy structure.

4.3 Summary of possible roles of different phases in creep response

The results presented in this study and in a recent similar study by the authors [2] allow to draw some important qualitative inferences on the possible roles of the different phases in the creep response of the studied Ti–6Al–4V alloy. These are summarised as follows.

i. The creep responses of Ti–6Al–4V alloys with equiaxed and duplex microstructures can be described by the same set of constitutive relationships (Equations (1)–(4)). For the former, the microstructure consists of equiaxed α-grains, with a relatively much lower

volume fraction of β-grains decorating the α-grain boundaries. In contrast, the duplex structure consists of equiaxed α- and lamellar α–β grains. In both equiaxed and duplex materials, the α-phase is predominant, and they show similar creep responses. It is reasonable to conclude that the β-phase, present in remote grains or coarse lamellae, plays a minor role. When creep is controlled by the dislocation activity in the α-phase, the α–β interfaces could possibly act as a strengthening source; however, the distance between these interfaces is too long for this mechanism to be effective.

ii. The creep response of the AM alloy annealed at 740 °C was shown to obey to the same set of constitutive equations [2]. In this case, the microstructure comprises approximately 90 % α-phase and small amounts of the β and α′-phases. This picture is fully consistent with the conclusion that creep is controlled by the dislocation activity in the α-phase, and the presence of relatively sparse widely spaced β-particles plays virtually no role.

iii. References [2] and [9], based on limited literature data, suggest that the creep response of an as-deposited AM material, whose initial microstructure is composed of α′-martensite, is almost equivalent to that of the uncrept alloy, in which the α-phase dominates. However, this is expected, because both the α and α′-phases have the same hcp structure but with quite different initial dislocation density and exposure to a high temperature during creep causes annealing of the martensitic structure.

iv. The volume fraction of the β-phase in the material annealed at 1050 °C was much higher than that in the alloy annealed at 740 °C. The β-phase volume fraction in the material annealed at 1050 °C was similar to that in the equiaxed and duplex alloys. A distinctive feature was the *bcc* phase, which here formed finely spaced lamellae. β-lamellae fragmentation occurred for long creep exposures at high temperatures following the initial annealing at 1050 °C. For the samples annealed at 740 °C, the fragmentation process was unnoticeable, because the β-phase did not form long lamellae as under the heat treatment at 1050 °C. The UTS after annealing was similar to those of the equiaxed and duplex

microstructures; therefore, the use of Equations (1)–(4) yields the same curves. However, the observed minimum creep rates were significantly lower for the former. Thus, the two most important features of the microstructure that could play a role in this behaviour are the fine spacing (a few hundreds of nanometres) of the β-phase lamellae and the presence of α_2-particles.

The findings summarised in this section suggest that modifying Equation (1)–(4) is necessary to describe the creep response of the alloy annealed at 1050 °C. Accordingly, the approach proposed by Barboza et al. [7], who introduced a threshold stress σ_0 (slightly ambiguous in nature) in the traditional Norton power-law equation describing the minimum creep rate dependence on temperature and stress, was tentatively used in [9]. This procedure simply involves substituting Equation (3) with

$$\sigma = \sigma_\rho + \sigma_{ss} + \sigma_0 = \sigma_\rho + \delta(\sigma - \sigma_0) + \sigma_0 \qquad (5)$$

Understandably, this is an approach of a phenomenological nature; however, it seems reasonable. In a first instance, suppose that the effect of α_2-particles can be neglected. In this case, the α–β interfaces could act as effective barriers for dislocation motion, and the strengthening mechanism could be quantified by σ_0. The effectiveness of these barriers depends on their spacing L. This behaviour can be tentatively described by an equation in the form,

$$\sigma_0 \propto \left(\frac{MGb}{L}\right)^p, \qquad (6)$$

where p is a constant. Thus, $\sigma_0 \cong 0$ in the equiaxed microstructure, where spacing L between the interfaces equals the α-grain size. Similarly, $\sigma_0 \cong 0$ in all cases in which the spacing is large, i.e., measurable on the micron scale (e.g., in lamellar grains where the α-lamellae are coarse).

The above scenario is likely to differ when the alloy is annealed above the β-transus temperature. In the latter case, the β-phase appears in the form of more closely spaced lamellae. As long as the spacing of the β-particles remains low, fragmentation of the lamellae does not necessarily significantly impair the alloy strengthening effect. This strengthening effect can be described by a

threshold stress $\sigma_0 \neq 0$. Additional α_2 precipitation, which introduces a typical particle-strengthening effect, also affects the magnitude of the threshold stress. This effect can compensate the softening effect, if any, due to the lamellae fragmentation.

Owing to the microstructural complexity described herein and limited physical models describing the strengthening effect of α–β interfaces and experimental information about the *L*-magnitude in crept materials, a quantitative correlation between microstructural features and σ_0 is presently impossible. Therefore, σ_0/G was calculated at a single temperature by fitting the experimental data. In particular, the preliminary results at 650 °C obtained in [9] were used as the basis for the analysis. In addition, first, it was arbitrarily assumed that σ_0/G did not change significantly with temperature. The other parameters for the calculation were the same as those used for the other Ti–6A–-4V alloy considered in [2]: Q_L = 303 kJ mol^{-1}, D_0 = 1.0 × 10^{-3} m^{2}s^{-1}, A = 40, and δ = 0.4. The UTS was assumed to be 1000 MPa, i.e., a value slightly higher than that obtained experimentally, to account for the strength reduction due to the surface being in the as-deposited state. In this regard, Figure 12 shows the experimental data for the alloys annealed at 740 °C and 1050 °C and the model curves obtained with the same parameters but σ_0/G = 0 and 1.19 × 10^{-3}, respectively. The correlation between the experimental and model results is good, except in the very high-strain rate region, where the model overestimates the strain rate. This deviation can be partly attributed to the underestimation of the UTS, in particularly at 500 °C, where a limited precipitation of the α_2-particles slightly increases the tensile strength.

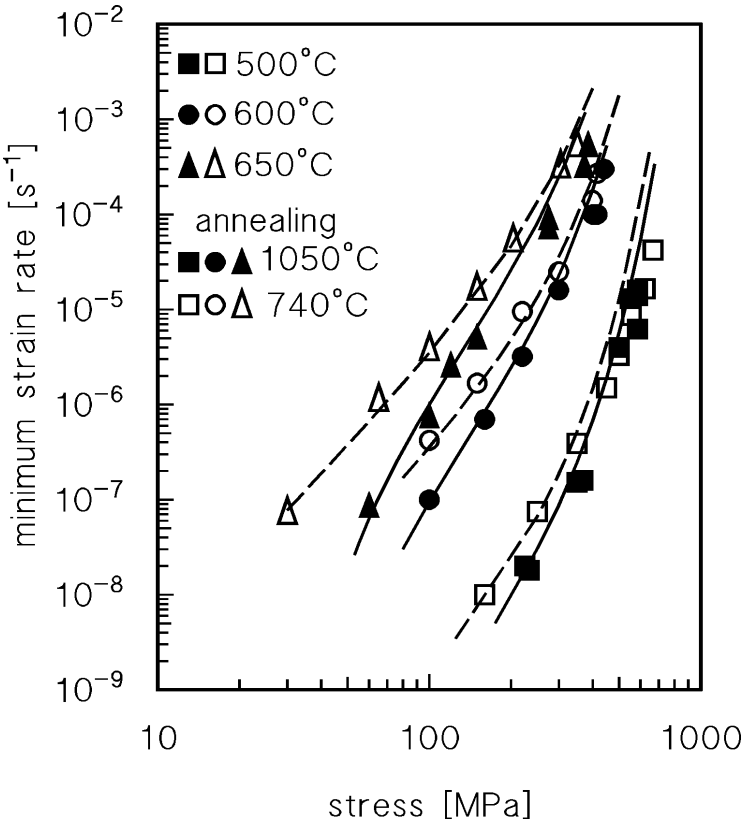

Figure 12. Experimental minimum creep rates for AM alloys annealed at 740 and 1050 °C and model curves with $\sigma_0/G = 0$ and 1.19×10^{-3}, respectively.

Based on Figure 12, the original concept of Barboza et al., i.e., the difference in creep behaviour can be described by introducing a threshold stress, provides a good phenomenological description of the creep response of the alloy with a Widmanstätten structure. The model can also rationalise the abnormal scatter observed in the literature creep data for alloys with such microstructures. The finesse of the Widmanstätten structure, i.e., the distance between the α–β interfaces, directly depends on the heat-treatment parameters (temperature, duration of annealing, and cooling rate). The distance between the α–β interfaces, in turn, determines the magnitude of the threshold stress. Furthermore, different amounts of the α_2-phase could be present in each case owing to the different thermal histories. Thus, the scatter among the creep data obtained by testing various batches of alloys annealed above the β-transus temperature, in this context, can be easily explained by simply

introducing small differences in the β- and α_2-phase volume fractions and distributions. This is a result of the heat-treatment processing parameters.

Figure 13 shows a representative case study. The curves obtained by combining Equations (1), (2), (4) and (5) with the same parameters used for Figure 12 and $\sigma_0/G = 2.0 \times 10^{-3}$ are compared with the experimental data from [7]. For six out of eight data points, the description is excellent. A deviation is observed only for a long time of exposure at 500 °C, i.e., in conditions where additional precipitation of the α_2-phase can be problematic. The model curve correctly estimates the minimum strain rate under 291 MPa at 500 °C with $\sigma_0/G = 4.85 \times 10^{-3}$. Thus, the model is correct, i.e., the microstructure undergoes considerable strengthening due to a reduction in L, presumably due to α_2-precipitation, during creep exposure.

Figure 13 shows speculative results because of the lack of experimental data on important features such as β- and α_2-phase volume fractions and distributions (i.e., on L) of that material. However, the threshold stress calculation in most creep studies was conducted by similar fitting procedures (see two examples in [24, 25]), which were typically not calculated by physical models of the dislocation/particle interaction. Thus, if it Figure 13 needs to be validated by microstructural studies, it unambiguously demonstrates that the proposed model is, in principle, appropriate for describing the creep response of the alloy annealed above the β-transus temperature.

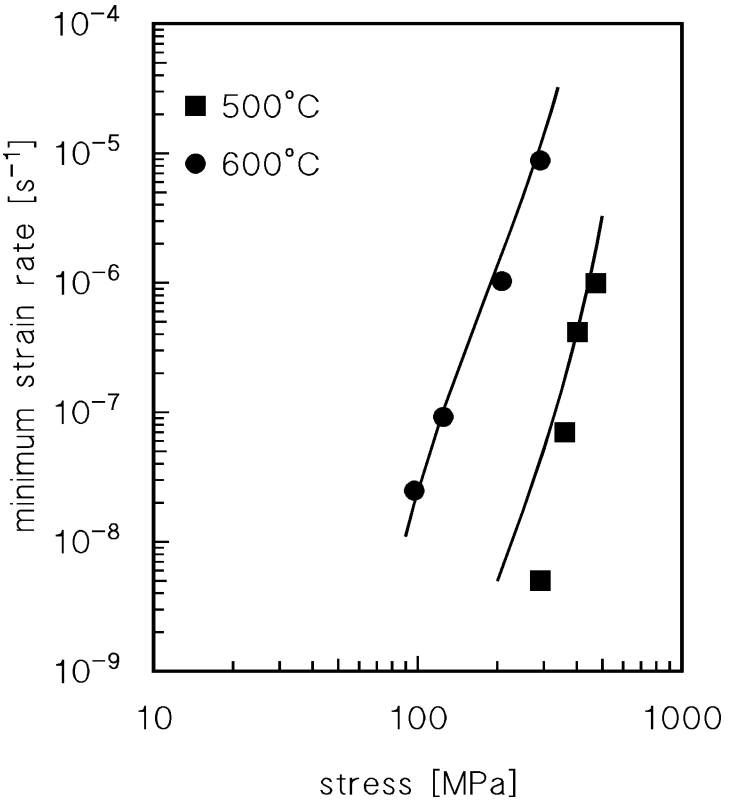

Figure 13. Model curves obtained with $\sigma_0/G = 2.0 \times 10^{-3}$ and experimental data from [7].

5. Conclusion

The creep responses of an AM Ti–6Al–4V alloy and annealed at 1050 °C were investigated at 500, 600, and 650 °C. The main findings of this study can be summarised as follows.

i. The alloy with a Widmanstätten microstructure typical of an alloy annealed above the β-transus temperature presented minimum creep rates lower than those of the same material annealed at lower temperatures.

ii. At a fine scale, the microstructure of the alloy annealed at 1050 °C, was characterised by the presence of finely spaced β-lamellae, which during creep exposure progressively underwent fragmentation. Nevertheless, at least for the relatively short durations investigated in the present study, the fragmented β-lamellae still formed a distribution of finely spaced particles.

iii. The presence of α_2-Ti_3Al particles was evident in all investigated microstructures, even at 650 °C, a temperature at which the presence of this phase is largely unexpected.

iv. The creep response of the alloy annealed at 1050 °C could be quantitatively described by introducing a threshold stress σ_0 in constitutive equations. These equations were previously used to analyse the creep responses of Ti–6Al–4V with equiaxed and duplex microstructures and the same alloy produced by additive manufacturing and annealed at 740 °C. This threshold stress can be considered as a quantification term for the strengthening role of both the α–β interfaces and α_2 particles. An excellent description could be obtained with a constant value of σ_0/G at the different temperatures, which suggests that the same hardening effect dominates between 500 and 650 °C.

v. For equiaxed, duplex, and annealed SLM-alloys, $\sigma_0/G = 0$ possibly suggests that the distance between the α–β interfaces is extremely long to be effective. This conclusion was supported by the experimental evidence obtained by studying the microstructure of the SLM-alloy annealed at 740 °C.

References

1. S. Liu, Y.C. Shin, Additive manufacturing of Ti6Al4V alloy: A review, Mater. Des. 164 (2019) 107552. https://doi.org/10.1016/j.matdes.2018.107552.

2. S. Spigarelli, C. Paoletti, M. Cabibbo, E. Cerri, E. Santecchia. On the creep performance of the Ti-6Al-4V alloy processed by additive manufacturing. Additive Manufacturing 49 (2022) 102520https://doi.org/10.1016/j.addma.2021.102520

3. S. Nishino, K. Shiozawa, Y. Aikawa, Effect of microstructure on creep and creep-fatigue behavior in Ti-6Al-4V alloy at elevated temperature, Mater. Sci. Sci. Res. Int. 4 (1997) 206–211. https://doi.org/10.2472/jsms.46.512.

4. G.F.C. Almeida, A.A. Couto, D.A.P. Reis, M. Massi, A.S. da Silva Sobrinho, N.B. de Lima, Effect of plasma nitriding on the creep and tensile properties of the Ti-6Al-4V alloy, Metals (Basel). 8 (2018) 0618. https://doi.org/10.3390/met8080618.

5. V.M.C.A. De Oliveira, M.C.L. Da Silva, C.G. Pinto, P.A. Suzuki, J.P.B. Machado, V.M. Chad, M.J.R. Barboza, Short-term creep properties of Ti-6Al-4V alloy subjected to surface plasma carburizing process, J. Mater. Res. Technol. 4 (2015) 359–366. https://doi.org/10.1016/j.jmrt.2015.05.006.

6. T. Sugahara, D.A.P. Reis, C. Moura Neto, M.J.R. Barboza, E.A.C. Perez, F. Piorino Neto, A.C.O. Hirschmann, The effect of Widmanstätten and equiaxed microstructures of Ti-6Al-4V on the oxidation rate and creep behavior, in: Mater. Sci. Forum, 2010: pp. 636-637 657-662. https://doi.org/10.4028/www.scientific.net/MSF.636-637.657.

7. M.J.R. Barboza, E.A.C. Perez, M.M. Medeiros, D.A.P. Reis, M.C.A. Nono, F.P. Neto, C.R.M. Silva, Creep behavior of Ti-6Al-4V and a comparison with titanium matrix composites, Mater. Sci. Eng. A. A428 (2006) 319–326. https://doi.org/10.1016/j.msea.2006.05.089.

8. V.M.C.A. Oliveira, A.M. Vazquez, C. Aguiar, A. Robin, M.J.R. Barboza, Nitride coatings improve Ti-6Al-4V alloy behavior in creep tests, Mater. Sci. Eng. A670 (2016) 357–368. https://doi.org/10.1016/j.msea.2016.06.041.

9. C. Paoletti, M. Cabibbo, E. Santecchia, E. Cerri, S. Spigarelli, Effect of Post-Processing Heat Treatments on Short-Term CreepResponse at 650 °C for a Ti-6Al-4V Alloy Produced by Additive Manufacturing, Metals 12 (2022) 1084. https://doi.org/10.3390/met12071084

10. A. Nespoli, N. Bennato, E. Villa, F. Passaretti. Study of anisotropy through microscopy, internal friction and electrical resis-tivity measurements of Ti-6Al-4V samples fabricated by selective laser melting, Rapid Prototyping Journal (2022) 28, https://doi.org/1060–1075. 10.1108/RPJ-06-2021-0151.

11. Xiao Li, Tian Sugui, Bao Xianyu, Chen Liqing, Creep properties and effect factors of hot continuous rolled Ti–6Al–4V alloy, Mater. Sci. Eng., A529 (2011) 452-458, ISSN 0921-5093, https://doi.org/10.1016/j.msea.2011.09.061.

12. M. Paghandeh, A. Zarei-Hanzaki, H.R. Abedi, Y. Vahidshad, On the warm temperature strain accommodation mechanisms of Ti–6Al–4V alloy holding different starting microstructures, J. Mater. Res. Technol., 14 (2021) 496-506, https://doi.org/10.1016/j.jmrt.2021.06.077.

13. Ying Zhang, Dongsheng Li, Xiaoqiang Li, Xiaochun Liu, Shiteng Zhao, Yong Li, Creep deformation and strength evolution mechanisms of a Ti-6Al-4V alloy during stress relaxation at elevated temperatures from elastic to plastic loading, J. Mater. Sci. Technol 126 (2022) 93-105, https://doi.org/10.1016/j.jmst.2022.02.042.

14. Jinlong Su, Xiankun Ji, Jin Liu, Jie Teng, Fulin Jiang, Dingfa Fu, Hui Zhang, Revealing the decomposition mechanisms of dislocations and metastable α' phase and their effects on mechanical properties in a Ti-6Al-4V alloy, Journal of Materials Science & Technology, 107 (2022) 136-148, https://doi.org/10.1016/j.jmst.2021.07.048.

15. D.G. Lee, S. Kim, S. Lee, Chong Soo Lee, Effects of microstructural morphology on quasi-1static and dynamic deformation behavior of Ti-6AI-4V alloy, Metall. Mater. Trans. A Phys. Metall. Mater. Sci. 32A (2001) 315–324. https://doi.org/10.1007/s11661-001-0263-y.

16. J. Tiley, T. Searles, E. Lee, S. Kar, R. Banerjee, J.C. Russ, H.L. Fraser, Quantification of microstructural features in α/β titanium alloys, Mater. Sci. Eng. A. A372 (2004) 191–198. https://doi.org/10.1016/j.msea.2003.12.008.

17. R. Sahoo, B.B. Jha, T.K. Sahoo, Effect of Microstructure on the Creep Properties of Ti–6Al–4V Alloys: An Analysis, Trans. Indian Inst. Met. Met 71 (2018) 1573–1582. https://doi.org/10.1007/s12666-018-1292-1.

18. J. Yu, M. Rombouts, G. Maes, F. Motmans, Material Properties of Ti6Al4V Parts Produced by Laser Metal Deposition, Phys. Procedia. 39 (2012) 416–424. https://doi.org/https://doi.org/10.1016/j.phpro.2012.10.056.

19. B. Vrancken, L. Thijs, J.P. Kruth, J. Van Humbeeck, Heat treatment of Ti6Al4V produced by Selective Laser Melting: Microstructure and mechanical properties, J. Alloys Compd. (2012) 177–185. https://doi.org/10.1016/j.jallcom.2012.07.022.

20.C. Qiu, N.J.E. Adkins, M.M. Attallah, Microstructure and tensile properties of selectively laser-melted and of HIPed laser-melted Ti-6Al-4V, Mater. Sci. Eng. A. A578 (2013) 230–239. https://doi.org/10.1016/j.msea.2013.04.099.

21.T.M. Mower, M.J. Long, Mechanical behavior of additive manufactured, powder-bed laser-fused materials, Mater. Sci. Eng. A. A651 (2016) 198–213. https://doi.org/10.1016/j.msea.2015.10.068.

22.S. Liu, Y.C. Shin, Additive manufacturing of Ti6Al4V alloy: A review, Mater. Des. 164 (2019) 107552. https://doi.org/10.1016/j.matdes.2018.107552.

23. S. Cao, R. Chu, X. Zhou, K. Yang, Q. Jia, C.V.S. Lim, A. Huang, X. Wu, Role of martensite decomposition in tensile properties of selective laser melted Ti-6Al-4V, J. Alloys Compd. 744 (2018) 357–363. https://doi.org/10.1016/j.jallcom.2018.02.111.

24. Y.Li, T.G.Langdon, A simple procedure for estimating threshold stresses in the creep of metal matrix composites, Scripta Mater 36 (1997) 1457-1460.

25.J.K. Benz, L.J. Carroll, J.K. Wright, R.N. Wright, T.M. Lillo. Threshold Stress Creep Behavior of Alloy 617 at Intermediate Temperatures, Metall Mater Trans 45A (2014) 3010-3022.